Effects of the cation and Si/Al ratio on CH3I adsorption by faujasite zeolites

B. Azambre, Mouheb Chebbi, Amal Hijazi

Effects of the cation and Si/Al ratio on CH_3I adsorption by faujasite zeolites: an experimental study

Bruno Azambre, Mouheb Chebbi, Amal Hijazi*

Laboratoire de Chimie et Physique-Approche Multi-Echelle des Milieux Complexes (LCP-A2MC- EA n°4362), Institut Jean-Barriol FR2843 CNRS, Université de Lorraine, Rue Victor Demange, 57500 Saint-Avold, France.

*corresponding author: e-mail address: bruno.azambre@univ-lorraine.fr

Keywords: silver, copper, ionic exchange, iodomethane, speciation, nuclear accident.

Abstract:

In this study, we aimed to investigate the effects of some specific zeolitic parameters on the retention properties of metal-exchanged faujasites (X and Y) for methyl iodide. In the first part, the nature of exchangeable cation (H^+, Na^+, Cu^+/Cu^{2+}, Ag^+, Pb^{2+}) is discussed. In order to link the materials properties with the adsorption behaviour, the state and location of the exchanged transition metals after calcination at 500°C were first investigated using N_2 sorptiometry at 77K, DRS-UV-Vis spectroscopy, XRD and FTIR of adsorbed CO and NO. Adsorption capacities at breakthrough and saturation were obtained from CH_3I breakthrough curves obtained at 100°C, this temperature being relevant to severe nuclear accident conditions. From the I/M ratio computed at saturation of the adsorbents by CH_3I vapors, it was found that the efficiency of iodine trapping follows the order $Cu^+/Cu^{2+} > Ag^+ >> Pb^{2+} > Na^+ > H^+$. This efficiency roughly followed the trend of the different cations to form stable MI_x precipitates from CH_3I. Nevertheless, for nuclear application, it was found that Ag/FAU are preferred over Cu/FAU, due to the propension of the latter to oxidize CH_3I to I_2, which slips out of the sorbent bed at 100°C.

The effect of the preparation method (ion-exchange vs impregnation) is then discussed for Ag/Y zeolites having different Si/Al ratio (2.5 and 40) but similar silver content (23 wt%). It is found that the silver oxidation state and silver dispersion have important effects on CH_3I adsorption/desorption.

1. Introduction

Silver zeolites are known for over 40 years to be efficient sorbents for the capture of iodine compounds (CH_3I and I_2 as main representatives) both in the contexts of severe nuclear accident and reprocessing of nuclear fuel [1-5]. Most of past and present R&D works in these fields have focused on silver mordenite zeolites (labelled Ag^0Z in many studies, and containing 9-15 wt% silver, also sold under the trademark *Ionex*) and also silver faujasites (type X) while little attention has been paid to other types of zeolites or frameworks [5-11]. Since the Fukushima disaster in 2011, many efforts were devoted to revisit the behavior of zeolitic sorbents because they were identified to present potentially satisfying performances even under severe accidental conditions [12-15]. Nevertheless, and before their potential application in FCVS-equipped nuclear power plants, several important issues remained to be solved about the effect of zeolitic parameters on their adsorption behavior, especially under extrapolated accident conditions (ionizing and oxidative conditions, presence of inhibitors (H_2O, CO_x, NO_x, H_2, chlorine compounds…), working temperature 25-250°C [16]…).

On the other hand, the iodine adsorption performances of zeolites containing other cations than silver, are comparatively poorly documented and were mostly obtained from old experimental studies [1-4]. The absence of relationships between the physico-chemical properties of these sorbents and their adsorption performances precluded a detailed understanding of the phenomena involved in sorption processes. Experimental reports could be found on the effect of the cation type in the case of I_2 capture [2-4] but no screening studies

exist for CH_3I. Owing to the differences existing in the chemical structures of I_2 and CH_3I, methyl iodide is always less easily adsorbed in comparison with molecular iodine [17]. For metal-exchanged zeolites, this stems probably from the higher activation energy needed to dissociate the C-I bond compared with the I-I bond, the latter almost proceeding without any activation barrier [18]. In a first approach, the affinity between iodine compounds and a given metal to form a stable metal iodide precipitate could be somewhat predicted by the Pearson-HSAB (Hard Soft Acid Base) theory [19]. Iodide (I-) being a soft base, it will react preferentially with soft acids (polarizable cations with large size and low charge) such as Cu^+, Ag^+, Au^+, Hg^+, Hg^{2+}, Pd^{2+}, Ti^{3+}, Tl^+, Pb^{2+}, Bi^{3+}…[20]. Nevertheless, other factors have to be taken into account during the design of a metal-containing sorbent for iodine, such as the volatility of the metal and MI precipitate and its water solubility, the stability of targeted metal oxidation state under handling conditions, the metal toxicity, and its cost/availability. In the case of zeolites, the ease of exchange reactions and the cation size are also further important criteria. Recently, some DFT studies conducted on different monovalent cation-exchanged faujasite and mordenite have shown new insights for the adsorption of both I_2 and CH_3I [21,22]. It was found that soft cations, such as Cu^+ and Ag^+, are able to adsorb iodine compounds with high adsorption energies, even in presence of some inhibitors (apart from CO and to a lesser extent NO) potentially present under severe accidental conditions. By contrast, hard cations such as H^+, Li^+, Na^+, K^+, exhibited much lower adsorption energies for CH_3I and I_2, as well as a greater affinity for water, which is rather in line with HSAB theory.

In order to bridge the gap between modeling and experimental studies, we aimed here to revisit the CH_3I sorption properties of X and Y faujasite zeolites bearing different types of exchangeable cations (H^+, Cu^{2+}, Ag^+, Na^+, Pb^{2+}). First, some insights on the textural and chemical properties of the corresponding zeolites will be given. Then, their CH_3I adsorption

properties will be investigated, namely using gas-phase experiments carried out at 100°C, which is a temperature representative of the conditions met in severe nuclear accident.

In a second part, the effect of the preparation method is discussed for silver faujasite Ag/Y zeolites with very different Si/Al ratio (*i.e.* bearing or not exchange sites). For some reason, the influences of silver oxidation state and its location (inside or outside the zeolitic framework) have been widely overlooked in the field of iodine capture by silver zeolites. However, it has been claimed, without much clue, that metallic silver nanoparticles (prepared by reduction in H_2) represent the preferred silver state for I_2 adsorption [4,23] on Ag^0Z mordenite, and that it exists an optimum size for which the adsorption is optimized. Nevertheless, this assumption has neither been comforted for other kinds of zeolites such as faujasites nor for CH_3I adsorption. Hence, in the present study, we propose to examine how CH_3I adsorption is impacted by the speciation of silver and its dispersion.

2. Experimental

2.1. Materials

Ion-exchanged zeolites. The parent NH_4/Y zeolite (Si/Al =2.5, *CBV 300*) was supplied by Zeolyst. For the study of the effect of the incorporated cation, a single ion-exchange was performed with the nitrate salts of Ag^+, Cu^{2+} and Pb^{2+} in order to obtain the Cu/Y, Ag/Y and Pb/Y zeolites. In the case of Ag/Y zeolite, all preparation steps as well as sample storage were carried out in the dark in order to avoid any photo-reduction of silver species. For each preparation, the solution containing the adequate metal nitrate (200 mL) is stirred with 2 g of the parent zeolite at 25°C and a pH of 5 for 24 hours. The concentration of each metal nitrate solution was chosen in order to obtain a theoretical content (provided an exchange degree of 100%) of approximately 10 wt% in each metal. Exchanged zeolites were then vacuum filtered, then rinsed with distilled water and then finally dried at 80°C overnight. Another Ag-

exchanged zeolite with a higher silver content (≈ 22.8 wt%) was prepared by three successive exchanges using the same procedure.

A 13X (NaX) zeolite (Si/Al =1.2, 60-80 mech, *20305*, Na^+ form) was purchased from Sigma Aldrich and also used for comparison purposes. Before use, all the zeolitic materials were calcined under air in a muffle furnace with a heating rate of 5°C/min from room temperature to 200°C (plateau of 1 hour) and then to 500°C (plateau of 2 hours). The H/Y (2.5) zeolite used for adsorption studies was obtained by calcination of the parent NH_4/Y material using the same procedure.

Ion-exchanged zeolites were denoted as: *xM/Type (Si/Al)* where *x* is the metal content in wt% and Type is either 13X or Y according to the kind of the parent material.

Impregnated zeolites. In order to study the effects of both the preparation method and the Si/Al ratio on the retention of methyl iodide, two other Ag/Y sorbents were obtained by Incipient Wetness Impregnation (IWI). For comparison purposes, the silver content in the impregnated zeolites was targeted to be also 23 wt%, which is similar to the mass percentage of the 3-times exchanged-silver zeolite (22.8Ag/Y (2.5)). Two different faujasite Y zeolites were used: (i) the same NH_4/Y zeolite as the one used for ion-exchange (Si/Al = 2.5, V_{porous} = 980 µL/g) and another H/Y zeolite with a much lower amount of exchange sites (Si/Al = 40, *CBV 780,* V_{porous} = 1080 µL/g). Once the pores saturated with the required amount of $AgNO_3$ solution, the samples were dried at 80°C overnight and further calcined at 500°C (procedure similar to ion-exchanged zeolites). The Ag-Y zeolites prepared by Incipient Wetness Impregnation (IWI) method were denoted as: 23Ag/NH_4-Y (2.5)_IWI and 23Ag/H-Y (40)_IWI.

2.2. Physico-chemical characterizations

Elemental analyses (Ag, Na, Cu, Pb, Al and Si) were performed either by AAS or ICP at the Service d'Analyses des Roches et des Minéraux (France).

Porosimetric properties were determined from N_2 adsorption isotherms recorded at 77K on an automated *Autosorb IQ* sorptiometer supplied by Quantachrome. Prior to each adsorption measurement, samples were outgassed *in situ* in vacuum at 80°C for 1h and then at 350°C for 6h to remove most of adsorbed impurities. Specific surface areas (S_{BET}) were determined using the BET equation ($0.05 < P/P_0 < 0.35$).

Powder X-ray diffraction (PXRD) measurements before and after test were carried out using a *Rigaku-Miniflex II* (Japan) with the CuKα radiation (λ= 0.15418 nm). PXRD patterns were recorded between 5 and 70° (2θ) using increments of 0.02° and a counting time of 2 s.

DRS UV-Vis spectra were collected on a *Varian Cary 4000 UV-Vis* spectrometer equipped with a double monochromator and *DRA900* integrating sphere. Spectra were registered between 200 and 800 nm, with a resolution of 2 nm and a scan rate of 600 $nm.min^{-1}$. Reflectance spectra were plotted in pseudo-absorbance mode, after correction with a Spectralon standard (taken as reference).

2.3. CH_3I gas-phase dynamic sorption experiments

The experimental setup devoted to CH_3I dynamic sorption was already described previously [13,14,24]. Briefly, CH_3I adsorption/desorption experiments were performed in a fixed-bed reactor (consisting of a quartz tube loaded inside a tubular furnace (Carbolite MTF with Eurotherm controller), using a sample mass of 200 mg, and a total flow rate of 150 $mL.min^{-1}$ (GHSV of 20000 h^{-1}). It can be divided schematically in three main parts: (i) the generation of a fixed and reproducible inlet concentration of CH_3I (1333 ppm/argon), (ii) the zeolitic bed (grain size between 200 and 630 µm) maintained between two pieces of quartz wool, and placed within a fixed bed reactor thermostated at 100°C for adsorption tests, (iii) the detection/quantification system composed by a Varian 4100 Excalibur FTIR spectrometer equipped with heated gas cell (C2 Cyclone Series – Specac, optical length = 2 m, V = 0.19 L). The formation of I_2 in the course of retention experiment was assessed qualitatively

(appearance of pink coloration) thanks to a cyclohexane liquid trap placed downstream the FTIR cell.

Prior to adsorption tests, the zeolitic materials were pretreated *in situ* under flowing argon at a temperature of 500°C (heating rate of 5°C.min^{-1}, plateau at 200 °C for 30 min and at 500 °C for 1 h). Adsorption tests were carried out at 100°C up to the total saturation of the zeolite bed by the incoming methyl iodide. Then, a degassing step was performed under argon at the same temperature in order to remove the physisorbed species. Finally, Temperature Programmed TPD experiments (heating from 100 to 500°C at a rate of 10°C.min^{-1} under argon) were performed to gain knowledge about the thermal stability of trapping.

Detailed procedures about experimental conditions and quantitative exploitation of gas-phase IR spectra were already given in our previous works [13].

3. Results and discussion

3.1. Effect of the cation type (H^+, Cu^{2+}, Ag^+, Pb^{2+}, Na^+) on the retention of methyl iodide by faujasite zeolites

3.1.1. Chemical and textural characteristics of exchanged faujasite zeolites.

The main textural properties of these materials as well as their cation contents are shown in Table 1.

Chemical properties. The H/Y (2.5) zeolite was prepared by calcination at 500°C of the commercial parent zeolite in ammonium form (see experimental). Elemental analyses on this sample revealed also the presence of residual sodium species (1.48 wt%), left in the material after synthesis. Previous characterization done by us and others on H/Y (2.5) [25], revealed that this zeolite has a rather moderate acidity (for instance compared with H/MOR or H/ZSM-5 zeolites), consisting of both Brönsted acid sites and defective Lewis acid sites. For the series of M/Y zeolites (M = Cu^{2+}, Ag^+ and Pb^{2+}), a single exchange was performed with the corresponding metal salts solutions (see experimental), leading to a rather low exchange

degree (Pb/Al = 0.11, Ag/Al = 0.26 and Cu/Al = 0.26) and a metal content inferior to 10 wt% in all cases (5.1wt% for Cu, 7.0wt% for Pb and 9.1wt% for Ag, Table 1).

Sample	% M	S_{BET} (m^2/g)	V micro (cm^3/g)	Cation speciation**
H/Y (2.5)	-	845	0.315	H^+ (Na^+)
10Na/X (1.2)	9.97	640	0.224	Na^+ (Mg^{2+}, Fe^{x+}, Ca^{2+}, K^+)
5.1Cu/Y (2.5)	5.10	806	0.270	Cu^{2+}(Cu^+)
7.0Pb/Y (2.5)	7.00	736	0.250	Pb^{2+}
9.1Ag/Y (2.5)	9.10	744	0.277	Ag^+, $Ag_n^{\delta+}$, $Ag°_m$
22.8Ag/Y (2.5)	22.8	704	0.253	Ag^+, $Ag_n^{\delta+}$, $Ag°_m$
23Ag/NH_4-Y (2.5)_IWI*	23.0	704	0.259	Ag^+, $Ag_n^{\delta+}$, $Ag°_m$, Ag° (traces)
H/Y (40)	-	871	0.200	H^+
23Ag/H-Y (40)_IWI	23.0	493	0.104	Ag° nanoparticles (diameter of 9.5 nm)

* IWI: Sample prepared by Incipient Wetness Impregnation method.
** as deduced from elemental analyses, XRD, DRS-UV-Vis spectroscopy and DRIFTS of adsorbed NO and CO.

Table 1 : Main physico-chemical characteristics of the investigated adsorbents.

These metal-exchanged zeolites bear also a certain concentration of acid sites in addition to cationic sites. These acid sites are formed during the thermal decomposition of the non-exchanged ammonium ions left after the ionic exchange process with transition cations and were observed for instance by DRIFTS in our recent study on Ag/Y sorbents [12]. A commercial Na/X zeolite (Si/Al = 1.2, fully in sodium form) was also used for comparison purposes. It had a sodium content of 9.97 wt% (Na/Al = 0.84) and bears also a certain amount of foreign cations, including Mg (1.75 wt%), Fe (0.9 wt%), Ca (0.57 wt%), K (0.36 wt%), Ti (0.19 wt%), P (0.08 wt%) and Mn (0.015 wt%)).

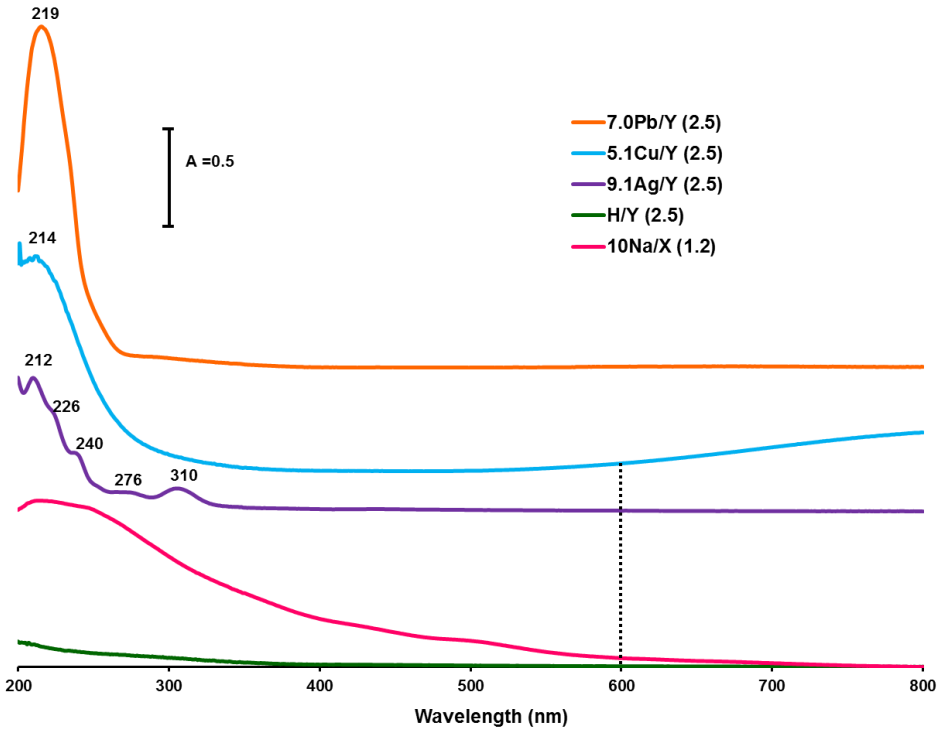

Figure 1 : DRS-UV-Vis spectra of metal-exchanged Y and X zeolites

The speciation of zeolitic metallic species was investigated by various methods, including XRD, DRS-UV-Vis spectroscopy and FTIR of adsorbed CO and NO. In line with the low exchange degrees, structural characterization of the investigated sorbents by XRD (Fig. S1 in ESI) did not reveal new crystalline phases after exchange with Cu, Ag and Pb. This confirms the good dispersion of transition metal species within the faujasite framework, as expected for exchange degrees below unity. Additional characterizations by DRS-UV-Vis and DRIFTS of molecular probes were already reported for Cu/Y [26] and Ag/Y [12] zeolites and only the most important aspects will be briefly summarized here. For both zeolites, a partial auto-reduction of exchanged species occurred following the thermal treatment performed at 500°C [27,28]. In the case of copper, both Cu^{2+} and Cu^{+} sites were found by DRIFTS of adsorbed CO and NO to coexist at different locations (exchange sites $S_{I'}$, S_{II} and S_{II}') after a pre-treatment under inert atmosphere [26,29], but Cu^{+} species were found to slowly re-oxidize under ambient conditions, conferring to the Cu/Y zeolite a pale blue color. The majority

presence of Cu^{2+} cations can be observed in Fig. 1 both from the d→d* transition above 600 nm [30] and the broad LMCT ($O^{2-} \rightarrow Cu^{2+}$) transition at 215-220 nm [31]. DRIFTS of adsorbed CO revealed that Ag^{+} cations mainly occupy sites S_{II} in the faujasite structures and to a lesser extent sites S_{III} [12]. As reported with more details in [32-34] , it is clearly evidenced by DRS-UV-Vis on Fig. 1, that these Ag^{+} cations (bands at 212 and 226 nm) at exchange positions coexist with intra-zeolitic clusters of $Ag_n^{\delta+}$ (240 and 276 nm) and Ag°_m types (310 nm). For 5.1Cu/Y and 9.1Ag/Y zeolites, auto-reduction processes are accompanied by the generation of new Brönsted acid sites in order to maintain the electroneutrality of the framework [27]. For the 7.0Pb/Y zeolite, the strong LMCT band observed in its DRS-UV-Vis spectrum at 219 nm (Fig. 1), is characteristic of the presence of Pb^{2+} embedded cations [35]. Although not studied for lead, it seems unlikely that auto-reduction processes also take place with this cation during calcination, because of its low reducibility compared with silver and copper. For 10.0Na/X, the broad absorptions observed in DR-UV-Vis spectrum in the ultraviolet and visible ranges (Fig. 1) are related not only to the presence of Na^{+}, but also to the presence of the oxides of other elements (Fe, Ti, Mg...).

Textural properties. For all Y-type zeolites, the N_2 adsorption isotherms measured at 77K (not shown here) were of type I, which is expected for purely microporous sorbents. From the textural characteristics reported in Table 1, it can be observed that the specific surface area and microporous volume were only slightly decreased after exchange with transition metallic species (Pb, Ag and Cu). Moreover, this decrease was rather logically function of the cation size ($Pb^{2+} > Ag^{+} > Cu^{2+} >> H^{+}$). By contrast, the Na/X zeolite also contains a small fraction mesopores (0.076 cm^3/g), and slightly lower textural properties than the Y-type zeolites (Table 1).

3.1.2. Sorption properties of exchanged faujasite zeolites

In order to assess the adsorption properties of metal-exchanged zeolites for methyl iodide, we used a similar methodology than that reported in our previous study [13]. The breakthrough curves obtained following the dynamic adsorption of CH_3I at 100°C are shown on Fig. 2. Before test, the exchanged zeolites were pretreated at 500°C under argon in order to eliminate the adsorbed moisture and other kinds of impurities. The adsorption capacities at breakthrough and saturation, I/M ratio and diffusional parameters obtained following the quantitative exploitation of these curves are given in Table 2.

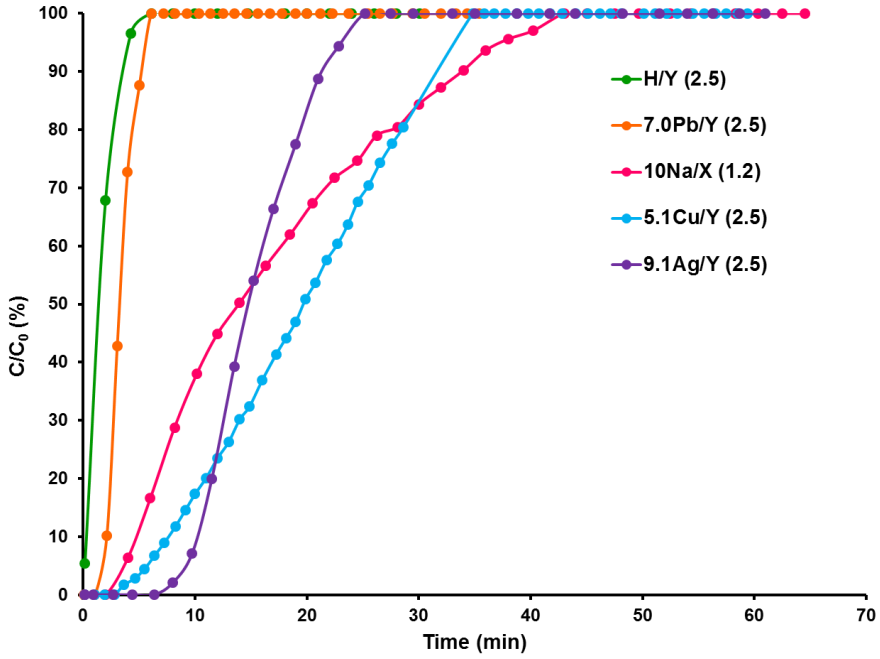

Figure 2 : Breakthrough curves obtained at 100°C during the dynamic adsorption of CH_3I (1333 ppm/Ar) on metal-exchanged zeolites of Y faujasite type

Although detailed studies devoted to the adsorption of CH_3I on protonated zeolites do not exist, our results showed that H/Y zeolite is not able to develop sufficiently strong interactions with CH_3I to promote stable storage at temperatures relevant to severe accident conditions (100 °C). Nevertheless, the involvement of Brönsted Si(OH)Al groups located in the supercages (as well as other defective OH groups) in the CH_3I trapping process over silver-exchanged faujasite at the same temperature was clearly evidenced previously [12]. By *in situ*

DRIFTS, a decrease in the concentration of OH groups was observed and this decrease was more pronounced for Ag/Y (bearing also protonic sites) than for H/Y.

Sample	Q_{sat} (mg/g)	$Q_{breakthrough}$ (mg/g)	L_T/L*	Global I/M
H/Y (2.5)	7	/	/	/
10Na/X (1.2)	92 ± 6	6 ± 1	0.92 ± 0.03	0.15
5.1Cu/Y (2.5)	114 ± 7	14 ± 2	0.83 ± 0.02	1.00
7.0Pb/Y (2.5)	18 ± 1	4 ± 1	0.73 ± 0.02	0.38
9.1Ag/Y (2.5)	87 ± 5	34 ± 4	0.64 ± 0.02	0.73
22.8Ag/Y (2.5)	223 ± 13	90 ± 10	0.70 ± 0.02	0.74
23Ag/NH_4-Y (2.5)_IWI	174 ± 10	70 ± 8	0.79 ± 0.02	0.57
23Ag/H-Y (40)_IWI	27 ± 2	15 ± 2	0.75 ± 0.02	0.09

$* \frac{L_T}{L} = \frac{(t_f - t_{5\%})}{t_f}$

Table 2 : The obtained CH_3I retention performances using the investigated metal loaded zeolites (C_0 = 1333 ppm, T=100°C).

On this basis, a cooperative mechanism between acidic OH groups and silver cations was proposed. It seems that, in presence of silver cations in the vicinity of Si(OH)Al groups, the C-I bond in the CH_3I adsorbed complex could be more easily dissociated, yielding a surface methoxy species and HI as products. The latter species reacts immediately with a silver cation giving AgI molecular species and a new Brönsted acid site [12,36]. In presence of exchanged cations, this mechanism could be generalized as follows: the zeolitic oxygen acts as a nucleophile by attacking the electron-deficient α-carbon on one end of the alkyl halide, while the framework cation (in this study Pb^{2+}, Cu^{x+}, Ag^{+}, Na^{+}) interacts with the halogen. As the halogen leaves, the alkyl carbocation (CH_3^{+}) is stabilized by the zeolitic oxygen to form the framework methoxy fragment ($Si(OCH_3)Al$).

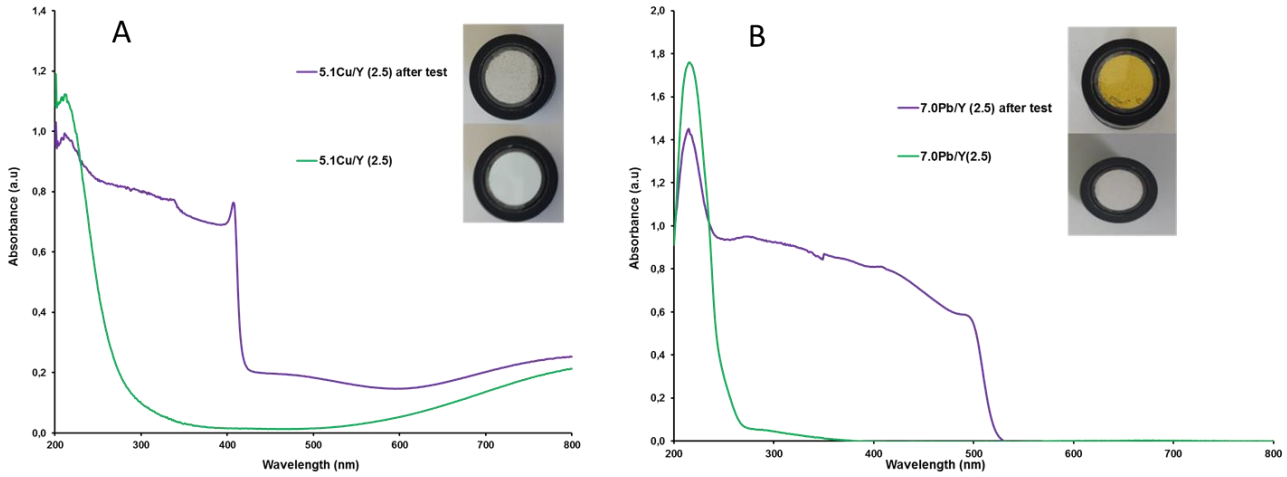

Figure 3 : DRS-UV-Vis spectra of (A) 5.1Cu/Y and (B) 7.0Pb/Y sorbents before and after CH_3I adsorption test performed at 100°C.

For the lead-exchanged zeolite (7.0Pb/Y (2.5)), the amounts adsorbed at saturation of the zeolite bed remained very low (Q_{sat} = 18 mg/g), only slightly higher than those measured for H/Y (Q_{sat} = 7 mg/g). Nevertheless, the formation of yellow-orange PbI_2 precipitates (Fig. 3(B)), corresponding to the absorption edge observed at 500-510 nm in DRS-UV-Vis spectrum was clearly evidenced after methyl iodide adsorption. In order to compare the efficiency of exchanged faujasite zeolites on a similar basis, the atomic I/M ratio can be calculated after saturation of the zeolite bed. For the 7.0Pb/Y (2.5) zeolite, this ratio was equal to 0.34. It is significantly lower than the expected one (I/Pb = 2), if all the lead cations were used to react with CH_3I to form PbI_2. Accordingly, the presence of unreacted Pb^{2+} cations is still visible in the DRS-UV-Vis spectrum at 219 nm (Fig. 3 (B)). Hence, this probably indicates both: (i) a limited accessibility of CH_3I to lead cations in the internal framework because of their large size (porosity blockage); (ii) a rather low adsorption/reaction efficiency. In that respect, it has to be recalled that dissociation of C-I bond is required in order to form PbI_2, but this reaction is thought be less efficient on lead (in comparison for instance with Ag^+, Cu^+ or Cu^{2+}) due to the known poor catalytic properties of this element.

By contrast, other forms of exchanged zeolites (Na/X, Ag/Y and Cu/Y) have much higher adsorption capacities at saturation (92, 87 and 114 mg/g, respectively, Table 2) despite some differences existing in their adsorption behavior. In our conditions, 34 min were needed in order to observe the breakthrough for the 9.1Ag/Y (2.5) zeolite (Fig. 2, Table 2). By contrast, the period of total decontamination (*i.e.* before filter breakthrough) is rather short for the 10Na/X (1.2) (6 min, Table 2) and 5.1Cu/Y (2.5) (14 min, Table 2) zeolites and the pronounced slope of the breakthrough curves indicates the existence of rather strong diffusional limitations for these zeolites [37]. Limitations in intracrystalline diffusion processes can be further assessed thanks to the adsorption capacities at breakthrough and the L_t/L ratio (indicative of the length of the mass transfer zone in zeolite bed) shown in Table 2.

For 10Na/X (1.2) zeolite, the I/Na ratio of 0.15 calculated at bed saturation witnesses of a rather small affinity of the sodium form for methyl iodide. Moreover, this ratio is probably overestimated since other elements (Mg, Fe, Ti, K, Mn…) were present in the commercial zeolite (see part 3.1.), and could also contribute to CH_3I adsorption. In the literature, it was reported that, despite rather similar adsorption capacities, the fraction of physisorbed I_2 (versus chemisorbed iodine) was much higher for Na/X (92 %) in comparison with Ag/X (39%) [4]. This can also be paralleled with our previous study where the forms of adsorbed CH_3I trapped by zeolitic materials were compared in terms of thermal stability [14]. It was shown that CH_3I adsorption by NaX zeolite was governed mainly by physisorption interactions (percentage of 39 %). In addition, the fraction trapped as NaI precipitate for NaX was significantly lower (26%) than the fraction trapped as AgI for Ag-X zeolites(57-76 %) [14]. Moreover, we also showed in a recent study that the coexistence of sodium and silver sites in Ag(Na)/X zeolites increases the total adsorption capacity of the materials in comparison with pure silver zeolites having similar silver content [13]. Although this confirmed the participation of sodium sites as secondary adsorption sites, the presence of

sodium had an apparent negative impact on the duration of the total decontamination period [13,14]. Taking also into account that NaI is very soluble in water (1840 g/L at 25°C [38]), zeolites in Na^+ form could not be considered as good sorbents for iodine in the context of severe accident.

By contrast with 10Na/X, 5.1Cu/Y and 9.1Ag/Y zeolites are characterized by I/M ratio of 1 and 0.72, respectively. First, it is clear that the accessibility of methyl iodide (kinetic diameter 0.5-0.6 nm [10]) to copper cations in the faujasite framework should be easier due to their smaller sizes (0.077 and 0.073 nm for Cu^+ and Cu^{2+} respectively [39]), as compared with Ag^+ (0.115 nm [39]) and also Pb^{2+} cations (0.119 nm [39]). Also, it has to be taken that intra-zeolitic silver clusters (of $Ag_n^{\delta+}$ and Ag°_m types) of larger size than Ag^+ cations are also present and could affect the diffusion behaviour, limiting the accessibility to some silver sites. On the other hand, much higher I/M ratio are measured for Cu/Y and Ag/Y, in comparison with Na/X and Pb/Y. This clearly evidence that copper and silver cations have a higher probability of reaction with CH_3I at the studied temperature (100 °C), which is in line with the results of a recent DFT study [21]. After-test characterization of the spent zeolites indicates the occurrence of CuI precipitated entities for Cu/Y (as revealed from the sharp absorption edge of colorless/greyish copper iodide *ca* 408 nm in DRS-UV-Vis spectrum, Fig. 3(A)). Moreover, the presence of residual Cu^{2+} species can be deduced from the absorptions near 200 nm and 700-800 nm. The origin of the weak absorption near 500 nm is less clear, as it could be assigned both to Cu° nanoparticles or physisorbed molecular iodine. The yellowish colour observed for Ag/Y (absorption edge at 430 nm) is explained by the presence of AgI precipitates (observed both by DRS-UV-Vis and XRD), as also outlined in our previous studies [12-14].

Although both CuI and AgI precipitates are thermally stable and almost insoluble in water [40-42], it is important to underline that some significant I_2 releases were observed in the

course of CH_3I sorption for the copper-exchanged zeolite. Although these emissions could not be quantitated by the FTIR detection used in our experimental setup, the formation of I_2 was undoubtly confirmed by the appearance of a pink-purple color in the cyclohexane liquid traps placed downstream the sorbent bed (Figure S2 in ESI).). To our knowledge, the catalytic oxidation of CH_3I by a copper-containing zeolite was never reported before. By contrast, such iodine release was never observed in the case of Ag/Y or for the other investigated zeolites. Obviously, this constitutes a major drawback for the use of a copper zeolite considering the nuclear context and the necessity to trap the most of radioactive iodine before its dissemination in environment.

Explanations for the odd behaviour of 5.1Cu/Y (2.5) zeolite can be depicted by the following equations:

$$Cu^{2+} + 2I^- \rightarrow CuI_2 \rightarrow 2CuI + \tfrac{1}{2} I_2 \qquad \text{(Eq. 1)}$$

$$Cu^{+} + I^- \rightarrow CuI \qquad \text{(Eq. 2)}$$

From Eq. (1), it can be seen that following the initial dissociation of CH_3I catalyzed by copper sites, CuI_2 could be formed. Owing to its known instability, it can decompose to stable CuI precipitate (observed by DRS-UV-Vis in Fig. 3(A)) while also producing I_2 as by-product. This should be the origin of molecular iodine emissions observed during the test at 100°C. On the other hand, the reaction of CH_3I with Cu^+ ions can lead directly to CuI formation without I_2 emission (Eq. 2). In the conditions of the gas-phase test at 100°C, Cu^+ species should at least partially coexist with Cu^{2+} because of some auto-reduction processes in Cu/Y zeolite during the *in situ* pretreatment performed at 500°C (see characterization part).

Results from gas-phase experiments at 100°C were also compared with those of liquid-phase tests performed at 10°C, with cyclohexane as the solvent. The adsorption capacities obtained at saturation of the sorbents are given in ESI (Table S1). Apart from silver zeolite, all the other exchanged M/Y zeolites (M = Na^+, Pb^{2+}, Cu^{2+}, H^+) exhibited much weaker adsorption

capacities (< 10 mg/g) in liquid-phase at 10°C than during gas-phase test at 100°C. By contrast, the 9.1Ag/Y zeolite maintained almost the same adsorption capacity (82 *vs* 87 mg/g, Table S3 and Table 2). Although it is difficult to explain these differences in detail, it seems that the dissociation of CH_3I proceeds with a lower activation barrier for the silver zeolite than for the other sorbents. For the Cu/Y zeolite, the explanation can be somewhat different. It is expected that the proportion of Cu^+ species towards Cu^{2+} species was probably much lower in liquid-phase tests, because no pre-treatment was carried out before contacting the sorbent with CH_3I. Accordingly, the adsorption capacity measured for Cu/Y in cyclohexane test is degraded. Here, it is worth noting that in practice, it is impossible to use copper zeolites exclusively in Cu^+ form, because the latter ions are unstable in air and spontaneously reoxidize to Cu^{2+} (providing a pale blue color to the zeolite, Fig. 3(A)). By contrast, silver cations do not undergo a change of oxidation state during CH_3I trapping. Hence, silver zeolites are strongly preferred for nuclear application and we will focus exclusively on this kind of sorbents afterwards.

3.2. Effect of the Si/Al ratio on silver state and CH_3I capture

Previously, we have reported that the adsorption capacities at saturation of silver-exchanged zeolites for CH_3I are mostly affected by their silver content rather than by the type of framework [13]. This time, we aimed to compare the behavior of silver faujasite zeolites (of the Y type), with similar silver content, but obtained from different Si/Al ratio and/or preparation methods (ion-exchange or impregnation). It is well-known from the rich literature devoted to silver supported catalysts (and other kinds of transition metals), that the preparation method could lead to significant differences in the dispersion/location and oxidation states for the incorporated silver [34,43,44]. In that case, both the conditions of thermal treatment/activation and the properties of the supporting oxide are very important. In

the presence of an oxide bearing exchange sites (e.g. zeolites with low Si/Al ratio), the incorporated silver could be stabilized as dispersed cations (or small clusters of a few atoms), whereas in the opposite case, large agglomerates of silver oxide or metallic silver are expected [34,43,44].

3.2.1. Effect of the Si/Al ratio on the physico-chemical characteristics of Ag/Y zeolites with similar silver content (23 wt%).

The textural and chemical properties of Ag/Y sorbents obtained from impregnation (corresponding to labels IWI in Table 1) are now compared with those of the ion-exchanged Ag/Y zeolite (22.8Ag/Y (2.5)) having identical silver content (≈ 23 wt%). For the ratio 2.5, the two sorbents remained white after drying and calcination, whereas the impregnated zeolite with Si/Al = 40 turned brown.

The two zeolites with similar Si/Al ratio (2.5), but obtained from different preparation methods, are compared first. The impregnated 23Ag/NH_4-Y (2.5)_IWI sorbent is characterized by almost similar textural properties than the ion-exchanged 22.8Ag/Y (2.5) zeolite (Ag/Al = 0.74), with S_{BET} = 704 m^2/g (-17 % vs the parent H/Y (2.5) zeolite, Table 1) and micropore volume 0.253 cm^3/g (-20 % vs the parent zeolite, Table 1). As revealed from the absence of any silver-related phase in the XRD pattern (Fig. 4 (B)), most of the silver in these two sorbents (with Si/Al = 2.5) is expected to be rather finely dispersed in the internal porosity. The DRS-UV-Vis spectra (Fig. 4 (A)) of both zeolites witness of the presence of high proportions of Ag^+ cations accompanied by the existence of charged and neutral intra-zeolite clusters resulted from auto-reduction processes [27]. A closer look to the relative intensities of the absorptions in the UV range indicates that the concentration of these clusters (and their size) is slightly higher for the impregnated zeolite than for the ion-exchanged one, which contains a slightly higher proportion of Ag^+. In addition, the plasmonic resonance of residual silver nanoparticles at 419 nm was solely observed for the impregnated zeolite,

confirming that the impregnation method led to a slightly lower degree of dispersion of the incorporated silver for a similar silver content. Nevertheless, at this low Si/Al ratio (2.5), the similarities observed in the textural and chemical characteristics of the ion-exchanged and impregnated zeolites could be reasonably understood considering that ion exchange reactions probably took place during impregnation due to the high concentration of exchange sites present within the pores (theoretical Cation Exchange Capacity (CEC) = 3.55 mmol/g).

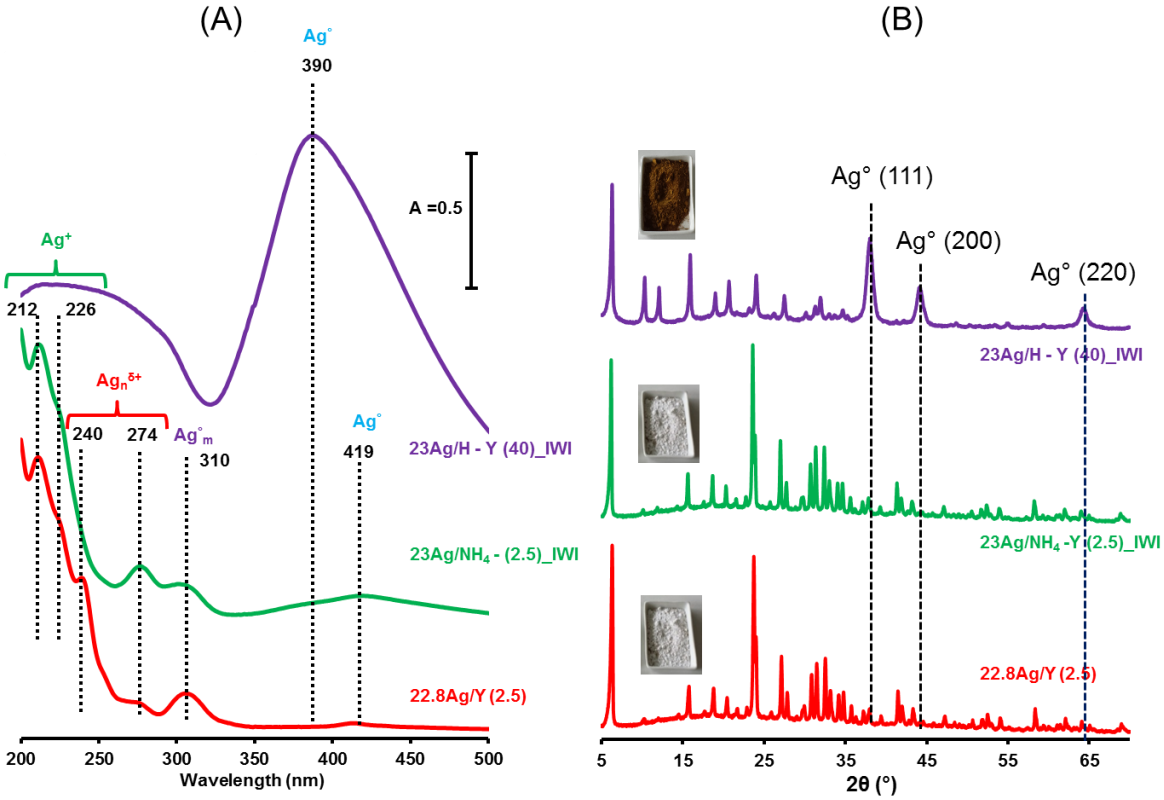

Figure 4 : Effect of Si/Al ratio and preparation method on the silver speciation by DRS-UV-Vis (A) and X-ray diffraction (B).

By contrast, the brown 23Ag/H-Y (40)_IWI impregnated sorbent was prepared from a parent H/Y(40) zeolite and has comparatively very few exchange sites due to its high Si/Al ratio (theoretical CEC = 0.295 mmol/g at Si/Al = 40). Since the computed Ag/Al ratio for 23Ag/H-Y (40)_IWI was clearly above 1 (Ag/Al = 6.4), most of the silver was expected to be present under agglomerated forms (as confirmed by the brown color of the zeolite, the two others remaining white). For 23Ag/H-Y (40)_IWI, XRD and DRS-UV-Vis analyses clearly

established the presence of metallic zerovalent nanoparticles on the external surface (the mean crystallite size computed from Debye-Scherrer equation was 9.5 nm) (Fig. 4 (A) & (B).

Overall, this impregnated zeolite at Si/Al = 40 showed a silver dispersion and speciation closer to those found for silver oxide supported catalysts bearing no or very few exchange sites. Nevertheless, the existence of a small fraction of Ag^+ cations and intrazeolitic clusters (< 3 wt%, as deduced from the CEC), as well as residual acid sites, has not to be discarded. The surface specific area of this sample is decreased by *ca* 25 %, as compared with the other Ag/Y zeolites (and by 43% if compare with the parent H/Y (40), Table 1), this being presumably due to the occlusion of some micropores by silver nanoparticles located at the external surface or at the pore mouth.

3.2.2. Effect of the Si/Al ratio on CH_3I retention in gaseous phase

Breakthrough curves obtained during the adsorption phase are shown on Fig. 4 for the ion-exchanged 22.8Ag/Y (2.5) and impregnated 23Ag/NH_4-Y (2.5)_IWI and 23Ag/H-Y (40)_IWI sorbents. Quantitative exploitation of adsorption data are shown in Table 2.

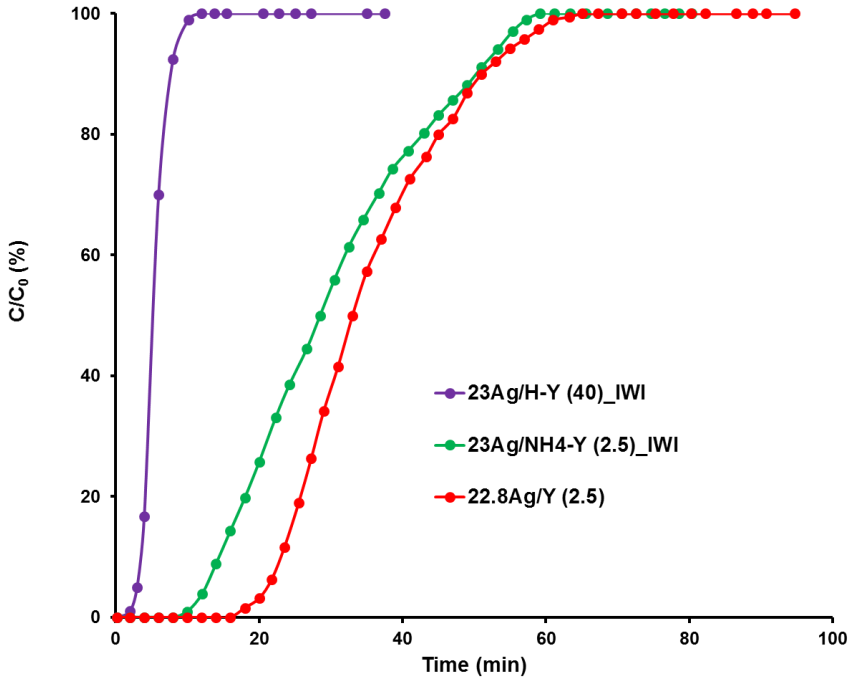

Figure 5 : CH_3I breakthrough curves obtained for 22.8Ag/Y (2.5), 23Ag/NH4-Y (2.5) and 23Ag/H-Y (40)_IWI (C0 = 1333 ppm, T = 100°C).

Immediately, it can be observed that the brownish 23Ag/H-Y (40)_IWI zeolite, bearing almost no exchange sites and exhibiting mostly silver nanoparticles on its outer surface, has much weaker CH_3I adsorption properties ($Q_{breakthrough}$ = 15 mg/g ; Q_{sat} = 27 mg/g, Table 2) than the ion-exchanged Ag/Y zeolite with lower Si/Al ratio (2.5) ($Q_{breakthrough}$ =90 mg/g ; Q_{sat} = 223 mg/g, Table 2). Since the silver content in both samples is similar, the superior retention properties of the ion-exchanged zeolite are here also obviously due to the high proportion of silver present in dispersed and oxidized state, namely as Ag^+ cations at exchange positions (see section 3.2.1.). In good agreement with characterization data, the retention behavior of the other impregnated zeolite (23 Ag/NH_4-Y (2.5)_IWI) resembles more to the ion-exchanged zeolite. Nevertheless, a slight decrease of the adsorption characteristics could be observed ($Q_{breakthrough}$ = 70 mg/g, Q_{sat} = 174 mg/g, Table 2) for the impregnated material, which is presumably due to a lesser proportion of Ag^+ cations and a higher content of agglomerated silver (see part 3.2.1.). Indeed, all our data indicate that the presence of dispersed silver in the +I oxidation state is preferred over zerovalent silver nanoparticles in order to enhance CH_3I adsorption. Accordingly, the I/Ag ratio that could be computed at saturation of the zeolite bed fall from 0.74 for 22.8Ag/Y (2.5) to 0.57 for 23Ag/NH_4-Y (2.5)_IWI and only to 0.09 for 23Ag/H-Y (40)_IWI (Table 2). For the latter zeolite, it means that only a very small part of the silver (< 10%) is used for the adsorption of CH_3I.

Sample	**Q sat (mmol/g)**	**Physisorbed CH_3I**		**Chemisorbed CH_3I**		**Iodine as precipitate***	
		(%)	Q_{phys} I (mmol/g)	**(%)**	Q_{chem} I (mmol/g)	**(%)**	Q_{AgI} (mmol/g)
22.8Ag/Y (2.5)	1.571 ± 0.094	**7 ± 2**	0.110 ± 0.007	**17 ± 4**	0.267 ± 0.080	**76 ± 4**	1.194 ± 0.012
23Ag/NH_4-Y (2.5)_IWI	1.226 ± 0.074	**12 ± 3**	0.147 ± 0.009	**14 ± 4**	0.172 ± 0.052	**74 ± 4**	0.907 ± 0.009
23Ag/H-Y (40)_IWI	0.190 ± 0.011	**58 ± 12**	0.110 ± 0.007	**3 ± 1**	0.006 ± 0.002	**39 ± 2**	0.074 ± 0.001

* obtained from mass balance using adsorption capacities at saturation expressed in mmol/g.

Table 3 : Molar amounts and fractions of iodine (in %) stored as physisorbed and chemisorbed CH_3I species, as well as AgI precipitates.

Once these zeolites were saturated by methyl iodide, they were first evacuated under argon at the same temperature (100°C) in order to estimate the fraction adsorbed as physisorbed species, *i.e.* the fraction that could be removed by a simple displacement of adsorption equilibrium due to different conditions. According to Table 3, the physisorbed fraction represents only 7% of the overall adsorbed capacity of the well-performing 22.8Ag/Y (2.5) ion-exchanged zeolite whereas it jumps to 58% for the impregnated 23Ag/H-Y (40)_IWI sorbent. However, this apparent difference has probably not to be directly related to the states and dispersions of silver in the different sorbents because physisorbed amounts were found to be approximately the same for all zeolites in terms of absolute values (Table 3). Hence, it simply reflects the possibility for a part of the incoming CH_3I molecules to be also weakly adsorbed on other sites than silver, such as acid sites for Si/Al = 2.5 or even through dispersive forces with the pore walls for Si/Al = 40. Since buried silver atoms in zerovalent nanoparticles do not participate in the formation of AgI entities for 23Ag/H-Y (40)_IWI, the contribution of weak adsorption phenomena to the total adsorption capacity is apparently enhanced for this sorbent.

Once the most weakly adsorbed species were eliminated, the spent zeolites were subjected to a thermal treatment under argon (v = 10°C/min) from the adsorption temperature (100°C) up to at least 600°C. During this treatment, CH_3I emissions were observed at 200-250°C (see desorption profiles in Figure S3). This fraction has to be assigned to chemisorbed CH_3I. During thermodesorption, catalytic degradation of adsorbed species also occurred, as witnessed by the presence of oxygenates (methanol, dimethylether), saturated hydrocarbons (CH_4, C_3H_8), olefins (C_2H_4, C_3H_6,) and CO in TPD profiles (Figure S3). As expected, these emissions overall increased with the amounts of CH_3I remaining adsorbed after the

evacuation phase at 100°C, in the order: 22.8Ag/Y (2.5) > 23Ag/NH_4-Y (2.5)_IWI >> 23Ag/H-Y (40)_IWI. It is interesting to note that the distribution of these by-products changed in function of the characteristics of the investigated silver zeolites. For the impregnated 23Ag/H-Y (40)_IWI zeolite, characterized by a high Si/Al ratio and bearing namely silver nanoparticles on the external surface, C_2 and C_3 hydrocarbons such as ethene, propane and propene were not observed (or present in too small amounts to be detected). By contrast, the emissions of acetaldehyde (not shown), methane and carbon monoxide were noteworthy higher on the silver zeolite with Si/Al = 40 than for the other zeolites (Si/Al = 2.5). In a previous study [12], it was shown by *in situ* DRIFTS that methyl iodide was adsorbed both in molecular form and as framework methoxy species (Si(OCH_3)Al) on the ion-exchanged Ag/Y zeolite. Methanol and dimethylether were formed via the methoxy route with regeneration of acid sites. Methane and higher hydrocarbons are produced from decomposition of the desorbing CH_3I (and perhaps also oxygenates) in a series of complex reactions involving acid and/or metallic sites, which are beyond the scope of this study. CO is probably produced from the partial oxidation of methane or adsorbed CH_3 fragments on silver nanoparticles. Overall, our results clearly showed that the state of silver and the Si/Al ratio of the zeolite (throughout the presence of acid sites) influence not only the amounts and forms of methyl iodide that could be adsorbed but also the CH_3I decomposition mechanism.

Since HI and I_2 were never observed in FTIR spectra or in cyclohexane traps, respectively, it is assumed afterwards that the dissociation of CH_3I should lead to the formation of AgI entities as the primary halogen-containing product. Hence, the impregnated materials with Si/Al = 2.5 and 40 were also characterized after CH_3I adsorption test by XRD (Fig. S4). Whereas the formation of AgI miersite (β-γ) phase (2Θ = 23.8;39.3;46.4°, JCPDS card n°78-0641) could clearly be evidenced for the lowest Si/Al ratio, the X-ray diffractogram of Ag/Y

with Si/Al = 40 still presented the characteristic *(111), (200), (220)* reflections of non-reacted Ag^0 nanoparticles (2Θ = 37.9,44.2,64.3, respectively) with the AgI phase being in minority.

In the following, the fraction of iodine trapped as AgI was calculated by subtracting the contributions from physisorbed and chemisorbed CH_3I to the total adsorption capacities of silver zeolites, as also explained in [14]. The fractions trapped as AgI were 76, 74 and 39 % for the 22.8Ag/Y (2.5), 23Ag/NH_4-Y (2.5)_IWI and 23Ag/H-Y (40)_IWI zeolites respectively (Table 3). Accordingly, the I/Ag ratio re-calculated for these zeolites without the contributions from physisorbed and chemisorbed CH_3I were equal to 0.56, 0.43 and 0.03, respectively (Table 3). In other words, this proves that only a very minor part of the silver (4 %) in the impregnated 23Ag/H-Y (40)_IWI sorbent is in a form suitable to produce AgI under the conditions of the present study. For this material, silver active sites should be located either at the surface of silver nanoparticles (with mean size 9.5 nm, as deduced from XRD measurements) or at Ag^+ cations or clusters in the internal porosity (at residual exchange sites).

Conclusions

In this paper, the effect of the cation (H^+, Cu^{2+}, Ag^+, Pb^{2+}, Na^+) on CH_3I adsorption was investigated experimentally for a series of exchanged faujasite Y and X zeolites. The characterization of these materials did not reveal the formation of bulk crystalline phases, as expected from their low exchange degrees. Owing to auto-reduction processes during the activation of the sorbents, the presence of silver clusters was found to co-exist with Ag^+ cations at exchange positions in Ag/Y whereas the presence of unstable Cu^+ species were noticed besides Cu^{2+} cation in Cu/Y. The quantitative exploitation of CH_3I breakthrough profiles measured at 100°C, led to the conclusion that the adsorption capacities at saturation follow the order $Cu^+/Cu^{2+} > Ag^+ >> Pb^{2+} > Na^+ > H^+$. The formation of stable precipitated

forms AgI, CuI and PbI_2 after adsorption test was observed either by DRS-UV-Vis or XRD for Ag/Y, Cu/Y and Pb/Y. Nevertheless, for nuclear application, silver faujasite is much preferred over copper faujasite, due to (i) a longer breakthrough/decontamination period; and (ii) the oxidation of some CH_3I to I_2 catalyzed by Cu/Y. The latter reaction occurs following the decomposition of an unstable CuI_2 intermediate, which releases molecular iodine out of the sorbent bed at 100°C.

For the first time, the effect of silver speciation and dispersion on CH_3I adsorption was investigated. This study was made possible by the comparison of the physico-chemical and adsorption properties of three Ag/Y zeolites having similar silver content (23 wt%), but which could be distinguished from their Si/Al ratio (2.5 or 40) and/or their preparation method (ion-exchange vs impregnation). It was found that low Si/Al ratio are essential in order to maintain a high amount of Ag^+ species at exchange positions in the faujasite framework, the preparation method being almost not influential in that respect. Dispersed Ag^+ species were found to be the most desirable silver form to trap CH_3I with a good use of silver and a high percentage trapped as stable AgI precipitate (fraction ≈ 75% at 100°C). By contrast, in absence of an appreciable amount of exchange sites (Si/Al = 40), metallic zerovalent silver nanoparticles are formed in high proportion and were found from after-characterization tests to be almost unaffected by CH_3I retention, resulting in inefficient trapping. These findings are expected to be important towards an optimal design of zeolitic sorbents for iodine capture.

Competing interests statement

The authors have no competing interests to declare

Acknowledgments

The research leading to these results was partly funded by the European Atomic Energy Community's (Euratom) Seventh Framework Programme FP7/2007-2013 under grant

agreement n° 323217. This work has been also supported by the French State under the program "Investissements d'Avenir" called MIRE, managed by the National Research Agency (ANR) under grant agreement n° ANR-11-RSNR-0013-01.

References

[1] W.J. Maeck, D.T. Pence and J.H. Keller, "A Highly Efficient Inorganic Adsorber for Airborne Iodine Species (Silver Zeolites Development Studies)." Idaho Nuclear Corporation IN-1224, 1969.

[2] D.T. Pence, and W.J. Maeck, "Silver Zeolite: Iodine Adsorption Studies." Idaho Nuclear Corporation, IN-1363, 1969.

[3] D.T. Pence, F.A. Duce, and W.J. Maeck, "Developments in the Removal of Airborne Iodine Species with Metal Substituted Zeolites", Proceedings of the 12th AEC Air Cleaning Conference, Tennessee (USA), August 28-31, 1972.

[4] B.A. Staples, L.P. Murphy, T.R. Thomas, "Airborne elemental iodine loading capacities of metal zeolites and a dry method for recycling silver zeolites", Proceedings of the 14th ERDA Air Cleaning Conference 1, 363-380, 1976.

[5] D.T. Pence, F.A. Duce, W.J. Maeck, "A Study of The Adsorption properties of metal zeolites for airborne iodine species", Proceeding of the 11th DOE/NRC Nuclear Air cleaning and Treatment Conference, Richland, Washington (USA), 31 August-3 September, 1970.

[6] T.R. Thomas, B.A. Staples, L.P. Murphy and J.T. Nichols, "Airborne elemental iodine loading capacities of metal exchanged zeolites and a method for recycling silver zeolites", Idaho National Engineering Laboratory, ICP-1119 (July 1977).

[7] R.T. Jubin, D.W. Ramey, B.B. Spencer, K.K. Anderson, S.M. Robinson, "Impact of Pretreatment and Aging on Iodine Capture Performance of Silver-Exchanged Mordenite-12314", WM2012 Conference, Phoenix, Arizona (USA), February 26-March 1, 2012.

[8] A.D. Belapurkar, K.A. Rao, N.M. Gupta, R.M. Iyer, Surf. Techn. 21 (1984) 263-272.

[9] B.S. Choi, G.I. Park, J.H. Kim, J.W. Lee, S.K. Ryu, Adsorption 7 (2001) 91-103.

[10] R.D. Scheele, L.L. Burger, C.L. Matsuzaki, "Methyl Iodide Sorption by Reduced Silver Mordenite." PNL-4489, Pacific Northwest Laboratory, 1983.

[11] K.W. Chapman, P.J. Chupas, T.M. Nenoff, J. Am. Chem. Soc. 132 (2010) 8897-8899.

[12] M. Chebbi, B. Azambre, L. Cantrel, A. Koch, J. Phys. Chem. C 120(33) (2016) 8694–18706.

[13] M. Chebbi, B. Azambre, L. Cantrel, M. Huvé, T. Albiol, Microporus Mesoporous Mater. 244 (2017) 137-150.

[14] B. Azambre, M. Chebbi, ACS Appl. Mater. Interfaces 9(30) (2017) 25194-25203.

[15] B. Azambre, M. Chebbi, O. Leroy, L. Cantrel, Ind. Eng. Chem. Res. 57(5) (2018) 1468–1479.

[16] L.E. Herranz, T. Lind, K. Dieschbourg, E. Riera, S. Morandi, P. Rantanen, M. Chebbi, N. Losch, "State of the Art Report : Technical Bases for Experimentation on Source Term Mitigation Systems." Passam-Theor-T04 [D2.1], 2013.

[17] S.H. Bruffey, R.T. Jubin, J.A. Jordan, Proced. Chem. 21 (2016) 293 – 299.

[18] J.E. Huheey, E.A. Keiter, and R.L. Keiter, Inorganic Chemistry, 4th ed. (1993)

[19] R.G. Pearson, Inorg. Chem. 27 (1988) 734-740.

[20] M. Guisnet, "Catalyse acido-basique." Article Techniques de l'ingénieur, j1210, 2005.
[21] M. Chebbi, S. Chibani, J.F. Paul, L. Cantrel, M. Badawi, Microporus Mesoporous Mater. 239 (2017) 111-122.

[22] S. Chibani, I. Medlej, S. Lebegue, J.G. Angyan, L. Cantrel, M. Badawi, ChemPhysChem, 18 (2017) 1642-1652.

[23] T.R. Thomas, B.A. Staples, L.P. Murphy, "Development of Ag°Z for bulk 129-I removal from nuclear reprocessing plants and PbX for 129-I storage", Proceedings of the 15th Nuclear Air Cleaning Conference, Boston, MA, 1978.

[24] M. Chebbi, B. Azambre, C. Volkringer, T. Loiseau, Microporus Mesoporous Mater. 259 (2018) 244-254.

[25] B. Azambre, A. Westermann, G. Finqueneisel, F. Can, J.D. Comparot, J. Phys. Chem. C 119 (2014) 315-331.

[26] A. Westermann, B. Azambre, M. Chebbi, A. Koch, Microporous Mesoporous Mater. 230 (2016) 76-88.

[27] M.D. Baker, G.A. Ozin, J. Godber, J. Phys. Chem. 89 (1985) 305-311.

[28] E. Sayah, D. Brouri, P. Massiani, Catal. Today 218-219 (2013) 10-17.

[29] G.T. Palomino, S. Bordiga, A. Zecchina, G.I. Marra, C. Lamberti, J. Phys. Chem. B 104 (2000) 8641-8651.

[30] B. M. Abu-Zied, Microporous Mesoporous Mater. 139 (2011) 59-66.

[31] S.A. Yashnik, Z.R. Ismagilov, V.F. Anufrienko, Catal. Today 110 (2005) 310-322.

[32] E. Sayah, D. Brouri, Y. Wu, A. Musi, P. Da Costa, P. Massiani, Appl. Catal. A Gen. 406 (2011) 94-101.

[33] S.G. Aspromonte, M.D. Mizrahi, F.A. Schneeberger, J.M.R. Lopez, A.V. Boix, J. Phys. Chem. C 117 (2013) 25433-25442.

[34] R. Bartolomeu, B. Azambre, A. Westermann, A. Fernandes, R. Bertolo, H. Issa Hamoud, C. Henriques, P. Da Costa, Appl. Catal. B Environ. 150-151 (2014) 204-217.

[35] Y.H. Yeom, Y. Kim, K. Seff, J. Phys. Chem. B 101 (1997) 5314-5318.

[36] T. Bucko, S. Chibani, J-F. Paul, L. Cantrel, M. Badawi, Phys. Chem. Chem. Phys 19 (2017) 27530-27543.

[37] J.M. Lopez, M.V. Navarro, T. Garcia, R. Murillo, A.M. Mastral, F.J. Varela-Gandia, D. Lozano-Castello, A. Bueno-Lopez, D. Cazorla-Amoros, Microporous Mesoporous Mater. 130 (2010) 239-247.

[38] A. Seidell, "Solubilities of inorganic and organic compounds c. 2.", D. Van Nostrand Company, 1919.

[39] R. D. Shannon, Acta Crystallogr A. 32 (1976) 751–767.

[40] S.W.H. Crouch, "Fundamentals of Inorganic Chemistry.", Brooks/Cole, 2004, pp. A-6 ISBN 978-0-03-035523-3.

[41] K.P. Anderson, E. A. Butler, E. M. Woolley, J. Phys. Chem, 78 (1974) 2244-2247.

[42] L.L. Burger, R.D. Scheele, K.D. Wiemers, "Selection of a Form for Fixation of Iodine-129." Pacific Northwest Laboratory, PNL-4045, 1981.

[43] J. Shibata, Y. Takada, A. Shichi, S. Satokawa, A. Satsuma, T. Hattori, J. Catal. 222 (2004) 368-376.

[44] S.G. Aspromonte, R.M. Serra, E.E. Miro, A.V. Boix, Appl. Catal. A Gen 407 (2011) 134-144.